Sliding Ferroelectric Control of Unconventional Magnetism in Stacked Bilayers

Yongqian Zhu,[1,2] Mingqiang Gu,[3] Yuntian Liu,[3] Xiaobing Chen,[3,4] Yuhui Li,[3] Shixuan Du,[1,2,5,*] and Qihang Liu[3,4,†]
[1]Beijing National Laboratory for Condensed Matter Physics, Institute of Physics, Chinese Academy of Sciences, Beijing 100190, China
[2]University of Chinese Academy of Sciences, Chinese Academy of Sciences, Beijing 100190, China
[3]State Key laboratory of quantum functional materials, Department of Physics, and Guangdong Basic Research Center of Excellence for Quantum Science, Southern University of Science and Technology (SUSTech), Shenzhen 518055, China
[4]China Quantum Science Center of Guangdong-Hong Kong-Macao Greater Bay Area (Guangdong), Shenzhen 518045, China
[5]Songshan Lake Materials Laboratory, Dongguan 523808, China

(Received 24 February 2025; revised 26 May 2025; accepted 9 July 2025; published 1 August 2025)

The control of unconventional magnetism, which displays ferromagnetismlike properties with compensated magnetization, has drawn intense attention for advancing antiferromagnetic spintronics. Here, through symmetry analysis, we propose a general stacking rule, characterized by a connection operator linking two stacked bilayers, for controlling unconventional magnetism via sliding ferroelectricity. Such a rule enables the simultaneous switching of both electric polarization and nonrelativistic spin splitting or anomalous Hall effect in altermagnets, a class of collinear unconventional magnets. By comprehensively surveying the 80 layer groups, we identify all the stacking orders that allow for such two types of simultaneous switching. Furthermore, we extend the stacking rule to collinear compensated ferrimagnets, where the opposite-spin sublattices are not connected by any symmetry operator, yet the net magnetization remains zero. Combined with first-principles calculations, we demonstrate the sliding ferroelectric control of spin polarization and anomalous Hall effect in the altermagnetic AgF_2 and Fe_2MoSe_4 bilayers. Our Letter provides a symmetry strategy for achieving ferroelectric control of unconventional magnetism in bilayer systems and opens avenues for exploring new types of magnetoelectric coupling.

DOI: 10.1103/dmzg-ck2t

Introduction—Unconventional magnetism is broadly characterized by compensated magnetization yet exhibiting ferromagnetismlike properties, including spin splitting, anomalous Hall effect (AHE), quantum geometry, topological magnons, etc. [1]. Recent advances in classifying unconventional magnets according to spin-group symmetry have expanded the current understanding of magnetism [2–10]. A prominent example is altermagnetism, a type of collinear antiferromagnetism (AFM) that displays nonrelativistic spin splitting in momentum space [7,8,11–15]. The spin splitting originates from the collinear magnetic order rather than from relativistic spin-orbit coupling (SOC). Such magnetic order-induced spin polarization enables various spintronic applications, such as spin-polarized currents, spin-to-charge conversion, spin torques, and magnetoresistance [8,12,16–22]. Another representative category of unconventional magnetism is the AFM exhibiting the AHE [23–28], which enables the electrical readout of the magnetic state. In collinear and coplanar AFMs, the occurrence of the AHE necessarily requires SOC, while for noncoplanar AFM, it can originate solely from the magnetic order [29].

In AFM memories, controlling the two key properties of unconventional magnetism (i.e., spin splitting and AHE), typically by means of manipulating AFM moments by a spin torque, opens new possibilities for information writing [30,31]. While dissipationless spin-orbit torque can be driven by an in-plane electric field [32–34], manipulating AFM moments usually suffers from large energy dissipation as spin torque requires electric current in most cases [31,35–39]. Alternatively, sliding ferroelectricity provides an energy-efficient way [40] for controlling unconventional magnetism through a gate voltage, e.g., switching the spin polarization in altermagnets [41]. Stacking has been previously demonstrated as an effective approach for inducing either sliding ferroelectricity or altermagnetism in a wide range of two-dimensional (2D) materials [42–48]. However, a universal and efficient strategy for designing materials with coupled sliding ferroelectricity and multiple facets of unconventional magnetism is still lacking.

In this Letter, we propose a general symmetry rule for controlling unconventional magnetism via sliding ferroelectricity in bilayer systems. Such a symmetry rule can easily predict whether electric polarization and unconventional magnetism are coupled in stacked bilayers, based solely on the crystallographic layer group of their constituent

*Contact author: sxdu@iphy.ac.cn
†Contact author: liuqh@sustech.edu.cn

monolayers, the stacking operations and magnetic configurations of the bilayers. Combined with first-principles calculations, we demonstrate that in altermagnetic bilayer AgF_2, spin polarization and AHE can be independently controlled via sliding ferroelectricity. In contrast, simultaneous control of both spin polarization and AHE is achieved in altermagnetic bilayer Fe_2MoSe_4 and compensated ferrimagnetic bilayer CrI_3. Such simultaneous control provides an effective route to detect spin polarization switching through AHE measurements.

Symmetry rules for sliding ferroelectricity—For stacked bilayers, the existence of spontaneous electric polarization or unconventional magnetism is theoretically governed by their symmetries established on different group frameworks [43,46,49–52]. The switching of these properties between two bilayer configurations is determined by an operator that connects them [14,53–55], referred to as the connection operator. Obviously, the connection operator determines the coupling of ferroelectricity and unconventional magnetism. Based on these symmetry rules, we identify ferroelectric bilayers that can control unconventional magnetism as follows.

We first screen all the stacked bilayers with sliding ferroelectricity across all 80 layer groups. A bilayer system (B) consisting of a bottom layer (S) and a top layer (S') can be expressed as $B = S + S' = S + \hat{O}S$, where $\hat{O} = \{O|\boldsymbol{t}_o\}$ is a stacking operator transforming S into S' [43]. Here, O is the rotational part, and $\boldsymbol{t}_o$ is the translational part. A stacking operator $\hat{O}$ specifies a stacking order. We then consider a ferroelectric bilayer with the same lateral unit cell size as its constituent monolayers, possessing an out-of-plane electric polarization component(P). The symmetry operator ($\hat{R}$) of a bilayer system and the connection operator ($\hat{N}$) between two bilayer systems [see Fig. 1(a)] can be divided into two classes, $\hat{Q}^-$ and $\hat{Q}^+$ ($\hat{Q} = \hat{R}, \hat{N}$), which can and cannot reverse P, respectively. For each layer group of the constituent monolayer, we identify all the stacking orders with only $\hat{R}^+$ symmetries that permit P [43]. Then, we further screen those with switchable P through interlayer sliding (i.e., sliding ferroelectricity). For two bilayer configurations, opposite P requires a connection operator $\hat{N} = \hat{N}^-$, as shown in Fig. 1. By solving the equation set for $\hat{N}^-$ across 80 layer groups, we identify all the stacking orders with switchable P, as detailed in Supplemental Material, Sec. I [56]. Table I presents an example for layer groups No. 14–18 of the monolayer. A bilayer permits P when stacked with $O = m_{001}$ and $\boldsymbol{t}_o$ along the high symmetry line GB or CA. P can be switched when changing the stacking order from $\boldsymbol{t}_o$ to $-N^-\boldsymbol{t}_o + \boldsymbol{t}_0$ through interlayer sliding, where $\boldsymbol{t}_0$ represents the pure translational symmetry of the constituent monolayer.

Sliding ferroelectric control of spin polarization—Having obtained all stacked bilayers with switchable P, we turn to identify those with coupled ferroelectricity and unconventional magnetism. We first consider ferroelectric control of spin polarization in altermagnets. For 2D altermagnets, the symmetry $\hat{R}$, that connects two sublattices with opposite spins, cannot be a translation $\boldsymbol{t}$, inversion $\bar{1}$, rotation 2_{001}, or any of their combinations [42,57,82]. Because the considered ferroelectric bilayer contains only $\hat{R}^+$ symmetry, the requirement is reduced to $\hat{R}$ not being $\boldsymbol{t}$, 2_{001}, or their combinations. For example, altermagnetism is allowed in the ferroelectric bilayer with layer group $pb11$ (see Table I). Thus, we identify all the stacking orders allowing for altermagnetism from screened ferroelectric bilayers, as highlighted in Supplemental Material, Tables S1–S3 [56]. It is worth noting that the ferroelectric altermagnetic bilayers discussed here are fundamentally different from previously reported altermagnetic bilayers with $\hat{R} = \hat{R}^-$ (e.g., A-type AFM) [45–47], where $\hat{R}^-$ enforces a vanishing P. In contrast, the $\hat{R}^+$ symmetry in a bilayer system considered here originates from the constituent monolayer, a collinear antiferromagnet with different sublattices connected by $\hat{R}^+$.

Then, we further identify the ferroelectric altermagnetic bilayers with switchable spin polarization. We introduce the connection operator $\hat{N}_s$ [Fig. 1(a)], which is an operator of the spin space group [3,4,6,7,9]. The interlayer magnetic coupling includes two types: the Néel vectors of the two constituent monolayers are aligned in the opposite or the same direction [Figs. 1(a) and 1(b)]. We assume that the collinear magnetic moment of each ion remains unchanged

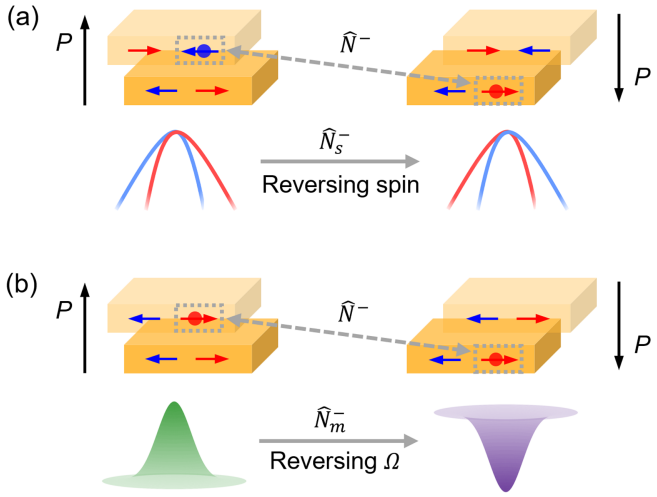

FIG. 1. Schematic diagrams of (a) configurations (upper) and bands (lower), (b) configurations (upper) and Berry curvatures (lower) of ferroelectric altermagnetic bilayers. The red and blue colors of arrows (lines) denote the opposite magnetic moments (spins). The black arrow denotes P. For the two stacked bilayers in (a) or (b), one can be transformed into the other through interlayer sliding. The sliding is equivalent to applying a $\hat{N}^-$ transformation, which maps the top (bottom) layer of one bilayer to the bottom (top) layer of the other. The solid circles in gray dotted line boxes denote atoms connected by $\hat{N}^-$, which have opposite spins in (a) while the same spin in (b).

TABLE I. Stacking configuration of layer groups No. 14–18 for the sliding ferroelectric control of spin polarization and AHE. $G_S(G_B)$ denotes the layer group of the monolayer (bilayer); $p2/m11$ and $p2_1/m11$ in G_S correspond to $pm11$ in G_B, $p2/b11$ and $p2_1/b11$ in G_S correspond to $pb11$ in G_B, and $c2/m11$ in G_S corresponds to $cm11$ in G_B. $\boldsymbol{t}_o$ is represented by high symmetry lines GB and CA in the rectangular lattice, with $G=(0,0)$, $A=(\frac{1}{2},0)$, $B=(0,\frac{1}{2})$, and $C=(\frac{1}{2},\frac{1}{2})$. For $N_s^-(N_m^-)$, only the operators capable of switching the spin polarization (AHE) are listed. The candidate monolayers are screened from Ref. [57].

G_S (No.)	$\{O\|\boldsymbol{t}_o\}$	G_B	N^-	N_s^-	N_m^-	Candidates
$p2/m11(14)$						
$p2_1/m11(15)$		$pm11$	m_{001}	$\{2_\perp\|\|m_{001}\}$	m'_{001}	AgF_2, RuF_4,
$p2/b11(16)$	$\{m_{001}\|GB,CA\}$	$pb11$	2_{010}	$\{1\|\|2_{010}\}$	2_{010}	VF_4, OsF_4
$p2_1/b11(17)$		$cm11$				
$c2/m11(18)$						

under interlayer sliding. Consequently, for the two atoms with opposite spins connected by $\hat{N}^-$ [Fig. 1(a)], considering spin rotation, they are connected by $\hat{N}_s^-$, where the rotational part is given by $N_s^- = \{2_\perp||N^-\}$. Here, the $2_\perp$ indicates a twofold spin rotation along the axis perpendicular to the collinear magnetic moments. Under $N_s^- = \{2_\perp||N^-\}$ operation, the spin polarization distribution with respect to the momentum $s^{\mathrm{I}}(\boldsymbol{k})$ transforms into $s^{\mathrm{II}}(\boldsymbol{k}) = N_s^- s^{\mathrm{I}}(\boldsymbol{k}) = -s^{\mathrm{I}}[(N^-)^{-1}\boldsymbol{k}]$, where the superscripts I and II denote the two ferroelectric states connected by $\hat{N}_s^-$. Taking $N^- = m_{001}$ as an example, since $(m_{001})^{-1}\boldsymbol{k} = \boldsymbol{k}$ for any $\boldsymbol{k}$ point, the spin polarization across the entire Brillouin zone can be reversed under ferroelectric switching, i.e., $s^{\mathrm{II}}(\boldsymbol{k}) = -s^{\mathrm{I}}(\boldsymbol{k})$, as shown in Fig. 1(a) and Table I. Consequently, the connection operator N_s^-, which depends on N^- and the type of interlayer magnetic coupling, determines the spin polarization reversal. We find that for all the ferroelectric altermagnetic bilayers connected by N^- screened above, at least one type of interlayer magnetic coupling enables spin polarization reversal under ferroelectric switching.

Sliding ferroelectric control of anomalous Hall effect—Now, we discuss the ferroelectric control of another facet of unconventional magnetism, i.e., AHE in AFM. Distinct from spin splitting, the symmetry requirement for AHE in 2D systems is that the sign of Berry curvature (Ω) remains unchanged under any symmetry operation. We consider AHE in 2D altermagnets, indicating the necessity of SOC and the framework of magnetic group, a specific subgroup of spin group. To achieve AHE in antiferromagnets with symmetry-enforced zero magnetization, the magnetic configuration must not align along the out-of-plane direction, otherwise the symmetry operations connecting the opposite-spin sublattices will reverse the sign of Berry curvature and thus enforce a zero anomalous Hall conductivity [83]. We consider the in-plane magnetic configuration. Because 2_{001} symmetry of a 2D altermagnet connects only the same-spin sublattice, it will result in a $2'_{001}$ symmetry in the magnetic point group for the in-plane configuration, leading to a vanishing AHE. Hence, any altermagnetic bilayers with 2_{001} point-group symmetry should be ruled out. We screen all the stacking orders permitting AHE from the ferroelectric altermagnetic bilayers, as highlighted in Supplemental Material, Tables S1–S3 [56].

We further identify ferroelectric altermagnetic bilayers with controllable AHE, which requires a sign reversal of Berry curvature under ferroelectric switching [see Fig. 1(b)]. When considering SOC, the connection operator belongs to magnetic space groups and is denoted as $\hat{N}_m^-$. The collinear in-plane magnetic configuration imposes a constraint that $N_m^- \in \{m_{001}, m'_{001}, 2_\alpha, 2'_\alpha\}$, indicating that $N^- \in \{m_{001}, 2_\alpha\}$, where 2_α denotes a twofold rotation with the rotational axis along the in-plane α direction. The sign reversal of Berry curvature requires $N_m^- \in \{m'_{001}, 2_\alpha\}$ (see Table I). This condition can be satisfied for all the above-screened ferroelectric altermagnetic bilayers with AHE under an appropriate magnetic configuration. Specifically, $N_m^- = m'_{001}$ requires that the two atoms connected by $N^- = m_{001}$ have the same spin [see Fig. 1(b)]. On the other hand, $N_m^- = 2_\alpha$ requires the two atoms connected by $N^- = 2_\alpha$ have the same (opposite) spins when the spin is parallel (perpendicular) to the rotational axis of 2_α.

It is worth noting that AHE switching is not necessarily accompanied by a spin polarization switching in momentum space. According to our symmetry rules, for the stacking orders connected only by $N^- = 2_\alpha$, AHE and spin polarization can be switched simultaneously under ferroelectric switching. We mark all the stacking orders that allow for a simultaneous ferroelectric switching of both AHE and spin polarization, as highlighted in Supplemental Material, Tables S1–S3 [56].

Sliding ferroelectric control of unconventional magnetism in altermagnetic bilayer AgF_2 *and* Fe_2MoSe_4—We now apply the above symmetry analysis to realistic materials. Monolayer candidate materials that enable ferroelectric control of spin polarization and AHE via bilayer stacking, including AgF_2 [57], MF_4 (M = V, Ru, Os) [57], $V_2ClBrI_2O_2$ [57], Fe_2MX_4 (M = Mo, W; X = S, Se, Te) [58], $MnPSe_3$ [59], and $FeBr_3$ [57], are listed in Table I and Supplemental Material, Tables S1–S3 [56]. Among these, stacked bilayer AgF_2, MF_4 (M = V, Ru, Os), and $V_2ClBrI_2O_2$ allow for the ferroelectric control of spin polarization or AHE independently, whereas the others enable the ferroelectric simultaneous control of both spin polarization and AHE. We take two representative monolayers, AgF_2 and Fe_2MoSe_4, as illustrative examples.

The bulk phase of AgF_2 has been synthesized experimentally [84,85]. Monolayer AgF_2 is a d-wave altermagnetic candidate with the crystallographic layer group $p2_1/b11$ (No. 17) [17,57]. The sublattices with opposite spins are connected by symmetries $\{m_{100}|\frac{1}{2},\frac{1}{2}\}$ and $\{2_{100}|\frac{1}{2},\frac{1}{2}\}$. Although ferroelectricity is prohibited in monolayer AgF_2 due to the inversion symmetry, according to Table I, a bilayer

configuration allows for ferroelectric control of spin polarization or AHE independently when it is stacked with $O = m_{001}$ and $\boldsymbol{t}_o$ along the high symmetry line GB or CA. We next perform density functional theory (DFT) calculations on bilayer AgF_2. We denote B_1 and B_2 as bilayer configurations which are stacked with $\hat{O}_1 = \{m_{001}|(0.5, -0.16)\}$ and $\hat{O}_2 = \{m_{001}|(0.5, 0.16)\}$, respectively [see insets of Fig. 2(a) and Supplemental Material, Fig. S1 [56]]. Their interlayer magnetic coupling includes two types: type-I and type-II, as shown in the insets of Figs. 2(b) and 2(c), respectively. DFT calculations show that type-I is the magnetic ground state, with an energy 0.26 meV/f.u. lower than that of type-II. The stacking breaks inversion symmetry and transforms the layer group $p2_1/b11$ of the monolayer into $pb11$ of the bilayer, inducing a polarization P in $B_1(B_2)$ configuration [see Fig. 2(a)]. B_1 and B_2 are connected by $N^- = m_{001}$, enforcing exactly opposite P with the same amplitude (1.66 pC/m) for B_1 and B_2 configurations. The energy barrier for the ferroelectric switching from B_1 to B_2 is 17.1 meV/f.u.

In contrast to inversion symmetry breaking, stacking preserves the $\{m_{100}|\frac{1}{2}, \frac{1}{2}\}$ symmetry for $B_1(B_2)$ and thus inherits the altermagnetism, as shown in Fig. 2(b). The maximal spin splitting is 51 meV for the two highest occupied bands. B_1 and B_2 with the type-I magnetic configuration are connected by $N_s^- = \{2_\perp||m_{001}\}$, which enforces them to have opposite $\mathbf{k}$-dependent spin polarizations [Fig. 2(b)]. Therefore, the spin polarization can be switched by sliding ferroelectricity in bilayer AgF_2.

We next consider the SOC effect and discuss AHE in B_1 and B_2. By comparing the energies of $B_1(B_2)$ with the Néel vector aligned along [100], [010], and [001] directions, we find that the easy axis is along the [100] direction, as shown in the inset of Fig. 2(b). $B_1(B_2)$ has the magnetic point group $m' = \{1, m'_{100}\}$, which permits a nonzero anomalous Hall conductivity σ_{xy}. However, considering SOC, B_1 and B_2 are connected by $N_m^- = m_{001}$, which does not switch the sign of Berry curvature and thus cannot switch the AHE. Switching AHE requires $N_m^- = m'_{001}$, which necessitates tuning the magnetic state of $B_1(B_2)$ to the type-II configuration, as shown in the inset of Fig. 2(c). We take AgF_2 bilayers under a 4% biaxial tensile strain as an example, and denote B_{1s} and B_{2s} as the bilayer B_1 and B_2 under strain, respectively. For both B_{1s} and B_{2s}, the type-II magnetic configuration is the ground state (see Table S4 [56]). The easy axis remains along the [100] direction. While the sliding ferroelectricity is preserved under strain (see Fig. S2 [56]). B_{1s} and B_{2s} exhibit opposite anomalous Hall conductivities as their connection operator $N_m^- = m'_{001}$ reverses the sign of Berry curvature [see Figs. 2(c) and S2 [56]]. These results indicate that the AHE can be controlled by the sliding ferroelectricity in strained bilayer AgF_2.

Similar to monolayer AgF_2, monolayer Fe_2MoSe_4 is also an altermagnetic candidate with the layer group $p\bar{4}2m$ (No. 57) [58]. However, unlike AgF_2 bilayers connected by

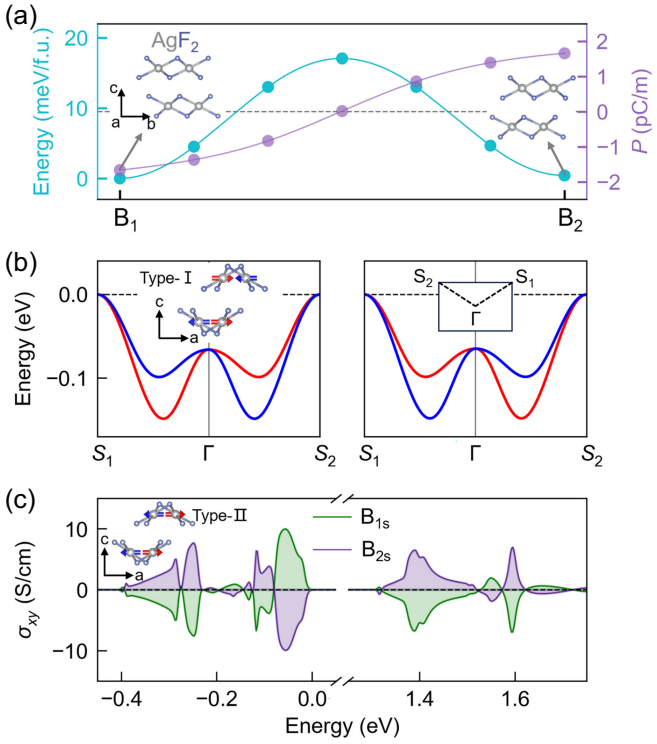

FIG. 2. (a) The energy barrier and the evolution of out-of-plane polarization along the sliding path between AgF_2 bilayers B_1 and B_2. The inset shows configurations of B_1 and B_2. (b) The two highest occupied bands of B_1 (left) and B_2 (right), calculated without considering SOC. The red and blue colors denote opposite spins. The Fermi level is set to zero. The left inset shows the type-I magnetic configuration, where red and blue arrows denote opposite magnetic moments. The right inset displays the Brillouin zone, where the high symmetry points $S_1 = (\frac{1}{2}, \frac{1}{2})$ and $S_2 = (-\frac{1}{2}, \frac{1}{2})$. (c) The anomalous Hall conductivities of B_{1s} and B_{2s}, calculated with considering SOC. The valence band maximum is set to zero. The inset shows the type-II magnetic configuration, where red and blue arrows denote the magnetic moment along [100] and $[\bar{1}00]$ directions, respectively.

$N^- = m_{001}$, Fe_2MoSe_4 bilayers allow for being connected only by $N^- = 2_{100}$ and thus enable spin polarization and AHE to be simultaneously switched via sliding ferroelectricity (see Supplemental Material, Table S2 [56]). We next perform DFT calculations on bilayer Fe_2MoSe_4. As shown in Fig. 3(a), we denote B_1 and B_2 as the two bilayer Fe_2MoSe_4 configurations which are stacked with $\hat{O}_1 = \{1|(\frac{1}{4}, \frac{1}{4})\}$ and $\hat{O}_2 = \{1|(-\frac{1}{4}, \frac{1}{4})\}$, respectively. The stacking transforms the layer group $p\bar{4}2m$ of the monolayer into $pm11$ of the bilayer, inducing a polarization P in B_1 (B_2) configuration. B_1 and B_2 are connected by $N^- = 2_{100}$, enforcing exactly opposite P with the same amplitude (0.14 pC/m) for them.

Figure 3(b) shows the same magnetic configuration for B_1 and B_2. In this magnetic configuration, they are connected by $N_s^- = \{2_\perp||2_{100}\}$ without considering SOC, and by $N_m^- = 2_{100}$ when SOC is included. As shown in

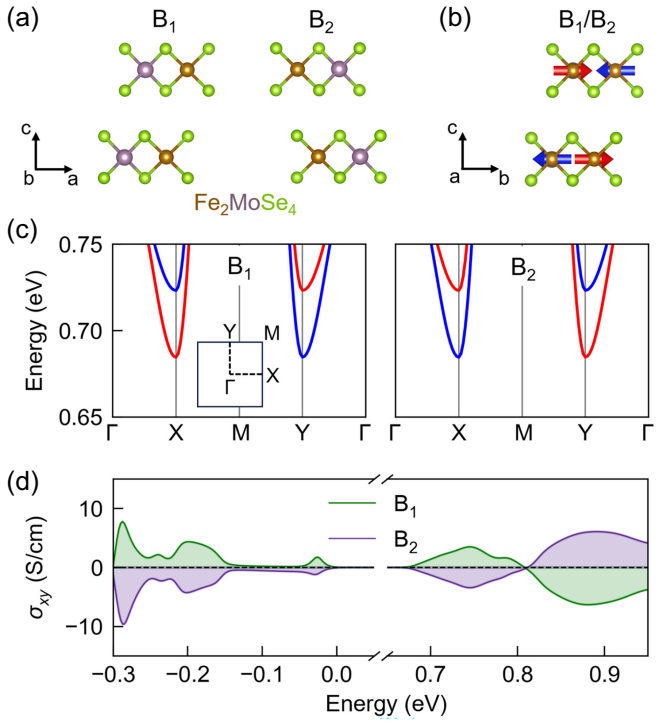

FIG. 3. (a) The configurations of Fe_2MoSe_4 bilayers B_1 and B_2. (b) The same magnetic configurations of B_1 and B_2. The red and blue arrows denote the magnetic moment along [010] and $[0\bar{1}0]$ directions, respectively. (c) The two lowest unoccupied bands of B_1 and B_2, calculated without considering SOC. The red and blue colors denote opposite spins. The inset displays the Brillouin zone. (d) The anomalous Hall conductivities of B_1 and B_2, calculated with considering SOC. The valence band maximum is set to zero.

Fig. 3(c), N_s^- enforces that B_1 and B_2 exhibit opposite $\mathbf{k}$-dependent spin splitting with the maximal value of 39 meV for the two lowest unoccupied bands. When SOC is included, B_1 and B_2 exhibit opposite anomalous Hall conductivities enforced by $N_m^- = 2_{100}$, as shown in Fig. 3(d). Therefore, unlike bilayer AgF_2, both spin polarization and AHE of bilayer Fe_2MoSe_4 can be simultaneously switched via ferroelectric switching. Given that AHE is more accessible to detect experimentally than spin polarization [35], the simultaneous control of spin polarization and AHE enables spin polarization switching to be more observable.

Generalized stacking rule for compensated ferrimagnets—We now generalize the stacking rule to collinear compensated ferrimagnet (CFiM) [86–89]. Unlike altermagnets, where zero net magnetization is enforced by symmetry, collinear CFiMs exhibit zero net magnetization due to appropriate electron filling in semiconducting or half-metallic states. We focus on collinear CFiM bilayers, which consist of two ferromagnetic monolayers with opposite spins. Such CFiM are permitted for all stacking orders that support sliding ferroelectricity, as listed in Supplemental Material, Tables S1–S3 [56]. Interestingly, in ferroelectric CFiM bilayers with out-of-plane magnetic configurations, both spin polarization and AHE can be simultaneously controlled via sliding ferroelectricity (see the Appendix). Candidate materials include experimentally synthesized monolayer CrI_3 [90], $CrGeTe_3$ [91], $MnBi_2Te_4$ [92,93], etc. Taking CrI_3 as an example, DFT calculations demonstrate that spin polarization and AHE in CFiM bilayer CrI_3 can be simultaneously switched via sliding ferroelectricity (see details in Supplemental Material, Sec. IV [56]).

Summary and discussion—Recent studies have proposed electric control of spin polarization in altermagnets [94–96]. Reference [94] introduces gate-field control of the spin degree of freedom in altermagnets based on spin-valley-layer coupling. The spin control relies on inducing opposite valley polarization, which requires a constant electric field and is thus volatile. Reference [95] has proposed controlling the existence of altermagnetism through the phase transition between antiferroelectric and ferroelectric states. Reference [96] has proposed ferroelectric control of the sign of spin polarization in altermagnets. Compared with these studies, our Letter extends the range of electric controllable functionalities from spin polarization to AHE, and, furthermore, the simultaneous control of both spin polarization and AHE. Moreover, we generalize the stacking rule beyond altermagnets to include another type of unconventional magnets, i.e., collinear CFiMs.

In fact, the general rule is applicable not only to collinear unconventional magnets (such as altermagnets and collinear CFiMs), but also to noncollinear and noncoplanar ones. Additionally, the rule can be extended beyond spin polarization and AHE to other spin-dependent properties (e.g., magneto-optical effects) that can be switched by the connection operator. Our Letter provides a general strategy for designing unconventional multiferroic bilayer systems and developing energy-efficient antiferromagnetic spintronic devices.

Acknowledgments—This work is supported by the National Key Research and Development Program of China (2022YFA1204100), the National Natural Science Foundation of China (62488201 and 12274194), Shenzhen Science and Technology Program (No. RCJC20221008092722009 and No. 20231117 091158001), the Innovative Team of General Higher Educational Institutes in Guangdong Province (2020KCXTD001), and Guangdong Provincial Quantum Science Strategic Initiative (GDZX2401002).

Data availability—The data that support the findings of this Letter are not publicly available. The data are available from the authors upon reasonable request.

[1] Q. Liu, X. Dai, and S. Blügel, Nat. Phys. **21**, 329 (2025).
[2] X. Chen, Y. Liu, P. Liu, Y. Yu, J. Ren, J. Li, A. Zhang, and Q. Liu, Nature (London) **640**, 349 (2025).
[3] X. Chen, J. Ren, Y. Zhu, Y. Yu, A. Zhang, P. Liu, J. Li, Y. Liu, C. Li, and Q. Liu, Phys. Rev. X **14**, 031038 (2024).
[4] Y. Jiang, Z. Song, T. Zhu, Z. Fang, H. Weng, Z.-X. Liu, J. Yang, and C. Fang, Phys. Rev. X **14**, 031039 (2024).
[5] J. Krempaský *et al.*, Nature (London) **626**, 517 (2024).
[6] P. Liu, J. Li, J. Han, X. Wan, and Q. Liu, Phys. Rev. X **12**, 021016 (2022).
[7] L. Šmejkal, J. Sinova, and T. Jungwirth, Phys. Rev. X **12**, 031042 (2022).
[8] L. Šmejkal, J. Sinova, and T. Jungwirth, Phys. Rev. X **12**, 040501 (2022).
[9] Z. Xiao, J. Zhao, Y. Li, R. Shindou, and Z.-D. Song, Phys. Rev. X **14**, 031037 (2024).
[10] Y.-P. Zhu *et al.*, Nature (London) **626**, 523 (2024).
[11] S. Hayami, Y. Yanagi, and H. Kusunose, J. Phys. Soc. Jpn. **88**, 123702 (2019).
[12] H.-Y. Ma, M. Hu, N. Li, J. Liu, W. Yao, J.-F. Jia, and J. Liu, Nat. Commun. **12**, 2846 (2021).
[13] I. Mazin, K. Koepernik, M. D. Johannes, R. Gonzalez-Hernandez, and L. Smejkal, Proc. Natl. Acad. Sci. U.S.A. **118**, e2108924118 (2021).
[14] L. Šmejkal, R. González-Hernández, T. Jungwirth, and J. Sinova, Sci. Adv. **6**, eaaz8809 (2020).
[15] L.-D. Yuan, Z. Wang, J.-W. Luo, E. I. Rashba, and A. Zunger, Phys. Rev. B **102**, 014422 (2020).
[16] H. Bai, L. Han, X. Y. Feng, Y. J. Zhou, R. X. Su, Q. Wang, L. Y. Liao, W. X. Zhu, X. Z. Chen, F. Pan, X. L. Fan, and C. Song, Phys. Rev. Lett. **128**, 197202 (2022).
[17] L. Bai, W. X. Feng, S. Y. Liu, L. Smejkal, Y. Mokrousov, and Y. G. Yao, Adv. Funct. Mater. **34**, 2409327 (2024).
[18] R. Gonzalez-Hernandez, L. Smejkal, K. Vyborny, Y. Yahagi, J. Sinova, T. Jungwirth, and J. Zelezny, Phys. Rev. Lett. **126**, 127701 (2021).
[19] M. Naka, S. Hayami, H. Kusunose, Y. Yanagi, Y. Motome, and H. Seo, Nat. Commun. **10**, 4305 (2019).
[20] M. Naka, Y. Motome, and H. Seo, Phys. Rev. B **103**, 125114 (2021).
[21] D. F. Shao, S. H. Zhang, M. Li, C. B. Eom, and E. Y. Tsymbal, Nat. Commun. **12**, 7061 (2021).
[22] L. Šmejkal, A. B. Hellenes, R. González-Hernández, J. Sinova, and T. Jungwirth, Phys. Rev. X **12**, 011028 (2022).
[23] H. Chen, Q. Niu, and A. H. MacDonald, Phys. Rev. Lett. **112**, 017205 (2014).
[24] J. Kübler and C. Felser, Europhys. Lett. **108**, 67001 (2014).
[25] N. Nagaosa, J. Sinova, S. Onoda, A. H. MacDonald, and N. P. Ong, Rev. Mod. Phys. **82**, 1539 (2010).
[26] S. Nakatsuji, N. Kiyohara, and T. Higo, Nature (London) **527**, 212 (2015).
[27] A. K. Nayak, J. E. Fischer, Y. Sun, B. Yan, J. Karel, A. C. Komarek, C. Shekhar, N. Kumar, W. Schnelle, J. Kübler, C. Felser, and S. S. P. Parkin, Sci. Adv. **2**, e1501870 (2016).
[28] L. Šmejkal, A. H. MacDonald, J. Sinova, S. Nakatsuji, and T. Jungwirth, Nat. Rev. Mater. **7**, 482 (2022).
[29] M. T. Suzuki, T. Koretsune, M. Ochi, and R. Arita, Phys. Rev. B **95**, 094406 (2017).
[30] V. Baltz, A. Manchon, M. Tsoi, T. Moriyama, T. Ono, and Y. Tserkovnyak, Rev. Mod. Phys. **90**, 015005 (2018).
[31] T. Jungwirth, X. Marti, P. Wadley, and J. Wunderlich, Nat. Nanotechnol. **11**, 231 (2016).
[32] X. Feng, W. Wu, H. Wang, W. Gao, L. K. Ang, Y. Zhao, C. Xiao, and S. A. Yang, arXiv:2402.00532.
[33] C. Xiao, H. Liu, W. Wu, H. Wang, Q. Niu, and S. A. Yang, Phys. Rev. Lett. **129**, 086602 (2022).
[34] C. Xiao, B. Xiong, and Q. Niu, Phys. Rev. B **104**, 064433 (2021).
[35] L. Han, X. Fu, R. Peng, X. Cheng, J. Dai, L. Liu, Y. Li, Y. Zhang, W. Zhu, H. Bai, Y. Zhou, S. Liang, C. Chen, Q. Wang, X. Chen, L. Yang, Y. Zhang, C. Song, J. Liu, and F. Pan, Sci. Adv. **10**, eadn0479 (2024).
[36] J. F. Scott, Nat. Mater. **6**, 256 (2007).
[37] E. Y. Tsymbal, Nat. Mater. **11**, 12 (2011).
[38] P. Wadley *et al.*, Science **351**, 587 (2016).
[39] K. L. Wang, J. G. Alzate, and P. Khalili Amiri, J. Phys. D **46**, 074003 (2013).
[40] E. Y. Tsymbal, Science **372**, 1389 (2021).
[41] W. Sun, W. Wang, C. Yang, R. Hu, S. Yan, S. Huang, and Z. Cheng, Nano Lett. **24**, 11179 (2024).
[42] R. He, D. Wang, N. Luo, J. Zeng, K. Q. Chen, and L. M. Tang, Phys. Rev. Lett. **130**, 046401 (2023).
[43] J. Ji, G. Yu, C. Xu, and H. J. Xiang, Phys. Rev. Lett. **130**, 146801 (2023).
[44] L. Li and M. Wu, ACS Nano **11**, 6382 (2017).
[45] Y. Liu, J. Yu, and C.-C. Liu, Phys. Rev. Lett. **133**, 206702 (2024).
[46] B. Pan, P. Zhou, P. Lyu, H. Xiao, X. Yang, and L. Sun, Phys. Rev. Lett. **133**, 166701 (2024).
[47] S. Zeng and Y.-J. Zhao, Phys. Rev. B **110**, 174410 (2024).
[48] W. Sun, H. Ye, L. Liang, N. Ding, S. Dong, and S.-S. Wang, Phys. Rev. B **110**, 224418 (2024).
[49] C. Bradley and A. Cracknell, *The Mathematical Theory of Symmetry in Solids: Representation Theory for Point Groups and Space Groups* (Oxford University Press, New York, 2010).
[50] W. Brinkman and R. J. Elliott, Proc. R. Soc. A **294**, 343 (1966).
[51] W. Brinkman and R. J. Elliott, J. Appl. Phys. **37**, 1457 (1966).
[52] D. B. Litvin and W. Opechowski, Physica (Utrecht) **76**, 538 (1974).
[53] Y. Zhu, J.-T. Sun, J. Pan, J. Deng, and S. Du, Phys. Rev. Lett. **134**, 046403 (2025).
[54] D.-F. Shao, J. Ding, G. Gurung, S.-H. Zhang, and E. Y. Tsymbal, Phys. Rev. Appl. **15**, 024057 (2021).
[55] T. Cao, D.-F. Shao, K. Huang, G. Gurung, and E. Y. Tsymbal, Nano Lett. **23**, 3781 (2023).
[56] See Supplemental Material at http://link.aps.org/supplemental/10.1103/dmzg-ck2t for details about group theory analysis, computational methods and the DFT results of bilayer AgF_2 and CrI_3, which includes Refs. [43,53,57–81].
[57] J. Sødequist and T. Olsen, Appl. Phys. Lett. **124**, 182409 (2024).
[58] Y.-Q. Li, Y.-K. Zhang, X.-L. Lu, Y.-P. Shao, Z.-Q. Bao, J.-D. Zheng, W.-Y. Tong, and C.-G. Duan, Nano Lett. **25**, 6032 (2025).
[59] Z. Ni, A. V. Haglund, H. Wang, B. Xu, C. Bernhard, D. G. Mandrus, X. Qian, E. J. Mele, C. L. Kane, and L. Wu, Nat. Nanotechnol. **16**, 782 (2021).

[60] M. I. Aroyo, A. Kirov, C. Capillas, J. M. Perez-Mato, and H. Wondratschek, Acta Crystallogr. Sect. A **62**, 115 (2006).
[61] M. I. Aroyo, J. M. Perez-Mato, C. Capillas, E. Kroumova, S. Ivantchev, G. Madariaga, A. Kirov, and H. Wondratschek, Z. Kristallogr. **221**, 15 (2006).
[62] M. Derzsi, K. Tokár, P. Piekarz, and W. Grochala, Phys. Rev. B **105**, L081113 (2022).
[63] S. L. Dudarev, G. A. Botton, S. Y. Savrasov, C. J. Humphreys, and A. P. Sutton, Phys. Rev. B **57**, 1505 (1998).
[64] L. Elcoro, B. Bradlyn, Z. Wang, M. G. Vergniory, J. Cano, C. Felser, B. A. Bernevig, D. Orobengoa, G. de la Flor, and M. I. Aroyo, J. Appl. Crystallogr. **50**, 1457 (2017).
[65] S. Fredericks, K. Parrish, D. Sayre, and Q. Zhu, Comput. Phys. Commun. **261**, 107810 (2021).
[66] J. Fu, M. Kuisma, A. H. Larsen, K. Shinohara, A. Togo, and K. S. Thygesen, 2D Mater. **11**, 035009 (2024).
[67] S. Grimme, J. Antony, S. Ehrlich, and H. Krieg, J. Chem. Phys. **132**, 154104 (2010).
[68] G. Henkelman, B. P. Uberuaga, and H. Jónsson, J. Chem. Phys. **113**, 9901 (2000).
[69] J. D. Hunter, Comput. Sci. Eng. **9**, 90 (2007).
[70] R. D. King-Smith and D. Vanderbilt, Phys. Rev. B **47**, 1651 (1993).
[71] G. Kresse and J. Furthmüller, Comput. Mater. Sci. **6**, 15 (1996).
[72] G. Kresse and D. Joubert, Phys. Rev. B **59**, 1758 (1999).
[73] K. Momma and F. Izumi, J. Appl. Crystallogr. **44**, 1272 (2011).
[74] S. P. Ong, W. D. Richards, A. Jain, G. Hautier, M. Kocher, S. Cholia, D. Gunter, V. L. Chevrier, K. A. Persson, and G. Ceder, Comput. Mater. Sci. **68**, 314 (2013).
[75] J. P. Perdew, K. Burke, and M. Ernzerhof, Phys. Rev. Lett. **77**, 3865 (1996).
[76] G. Pizzi *et al.*, J. Phys. Condens. Matter **32**, 165902 (2020).
[77] R. Resta, Ferroelectrics **136**, 51 (1992).
[78] R. Resta, Rev. Mod. Phys. **66**, 899 (1994).
[79] A. Togo, K. Shinohara, and I. Tanaka, Sci. Technol. Adv. Mater. **4**, 2384822 (2024).
[80] V. Wang, N. Xu, J.-C. Liu, G. Tang, and W.-T. Geng, Comput. Phys. Commun. **267**, 108033 (2021).
[81] Q. Wu, S. Zhang, H.-F. Song, M. Troyer, and A. A. Soluyanov, Comput. Phys. Commun. **224**, 405 (2018).
[82] S. Zeng and Y.-J. Zhao, Phys. Rev. B **110**, 054406 (2024).
[83] Y. Liu, J. Li, and Q. Liu, Nano Lett. **23**, 8650 (2023).
[84] P. Fischer, D. Schwarzenbach, and H. M. Rietveld, J. Phys. Chem. Solids **32**, 543 (1971).
[85] X. Xu, Y. Ma, T. Zhang, C. Lei, B. Huang, and Y. Dai, Nanoscale Horiz. **5**, 1386 (2020).
[86] J. Finley and L. Liu, Appl. Phys. Lett. **116**, 110501 (2020).
[87] S. K. Kim, G. S. D. Beach, K.-J. Lee, T. Ono, T. Rasing, and H. Yang, Nat. Mater. **21**, 24 (2021).
[88] Y. Liu, S. D. Guo, Y. Li, and C. C. Liu, Phys. Rev. Lett. **134**, 116703 (2025).
[89] L.-D. Yuan, A. B. Georgescu, and J. M. Rondinelli, Phys. Rev. Lett. **133**, 216701 (2024).
[90] B. Huang, G. Clark, E. Navarro-Moratalla, D. R. Klein, R. Cheng, K. L. Seyler, D. Zhong, E. Schmidgall, M. A. McGuire, D. H. Cobden, W. Yao, D. Xiao, P. Jarillo-Herrero, and X. Xu, Nature (London) **546**, 270 (2017).
[91] C. Gong, L. Li, Z. Li, H. Ji, A. Stern, Y. Xia, T. Cao, W. Bao, C. Wang, Y. Wang, Z. Q. Qiu, R. J. Cava, S. G. Louie, J. Xia, and X. Zhang, Nature (London) **546**, 265 (2017).
[92] Y. Deng, Y. Yu, M. Z. Shi, Z. Guo, Z. Xu, J. Wang, X. H. Chen, and Y. Zhang, Science **367**, 895 (2020).
[93] M. M. Otrokov, I. P. Rusinov, M. Blanco-Rey, M. Hoffmann, A. Y. Vyazovskaya, S. V. Eremeev, A. Ernst, P. M. Echenique, A. Arnau, and E. V. Chulkov, Phys. Rev. Lett. **122**, 107202 (2019).
[94] R. W. Zhang, C. Cui, R. Li, J. Duan, L. Li, Z. M. Yu, and Y. Yao, Phys. Rev. Lett. **133**, 056401 (2024).
[95] X. Duan, J. Zhang, Z. Zhu, Y. Liu, Z. Zhang, I. Žutić, and T. Zhou, Phys. Rev. Lett. **134**, 106801 (2025).
[96] M. Gu, Y. Liu, H. Zhu, K. Yananose, X. Chen, Y. Hu, A. Stroppa, and Q. Liu, Phys. Rev. Lett. **134**, 106802 (2025).

End Matter

Appendix: Generalized stacking rule for compensated ferrimagnets—In a collinear compensated ferrimagnet (CFiM), the opposite-spin sublattices are not connected by any symmetry operator. We focus on collinear CFiM bilayers, which consist of two ferromagnetic monolayers with opposite spins. Since the two monolayers cannot be connected by a symmetry, CFiM bilayers require breaking R^- symmetry, and thus they are permitted for all stacking orders that allow sliding ferroelectricity, as listed in Supplemental Material, Tables S1–S3 [56]. For two CFiM bilayers exhibiting sliding ferroelectricity, they are connected by N^-. Considering spin rotation, they are connected by $N_s^- = \{2_\perp||N^-\}$ because the top and bottom monolayers have opposite spins. $N_s^- = \{2_\perp||N^-\}$ enables switching of nonrelativistic spin polarization, indicating that all considered CFiM bilayers can exhibit sliding ferroelectric control of spin polarization.

We next consider the SOC effect and discuss the sliding ferroelectric control of AHE in CFiM bilayers. Specifically, we consider the ferroelectric CFiM bilayer with an out-of-plane magnetic configuration, which can host AHE since its symmetry permits the out-of-plane magnetization and thus permits a nonzero Berry curvature. The AHE can be switched under ferroelectric switching since the connection operator N_m^- can reverse the out-of-plane magnetization and thus reverse the Berry curvature. Therefore, for all ferroelectric CFiM bilayers with out-of-plane magnetic configuration and stacking orders listed in Tables S1–S3 [56], their spin polarization and AHE can be simultaneously controlled via sliding ferroelectricity.